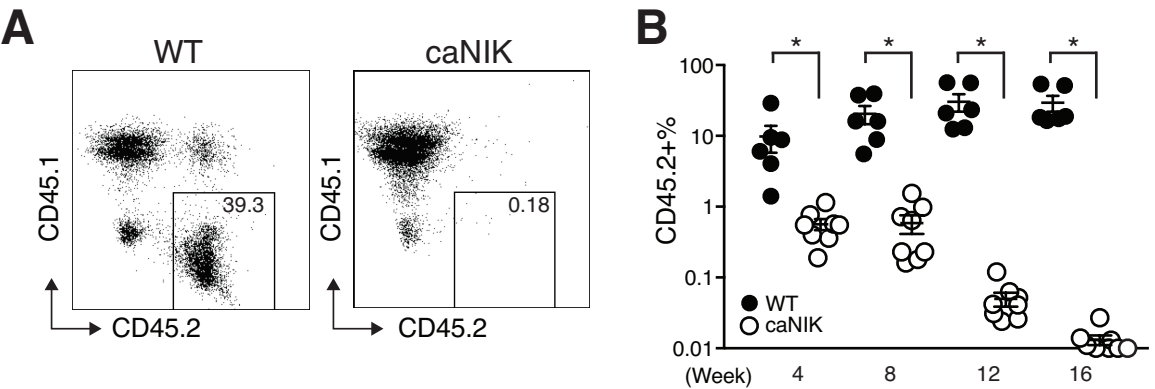

Supplemental Fig. 1 Zhao et al.

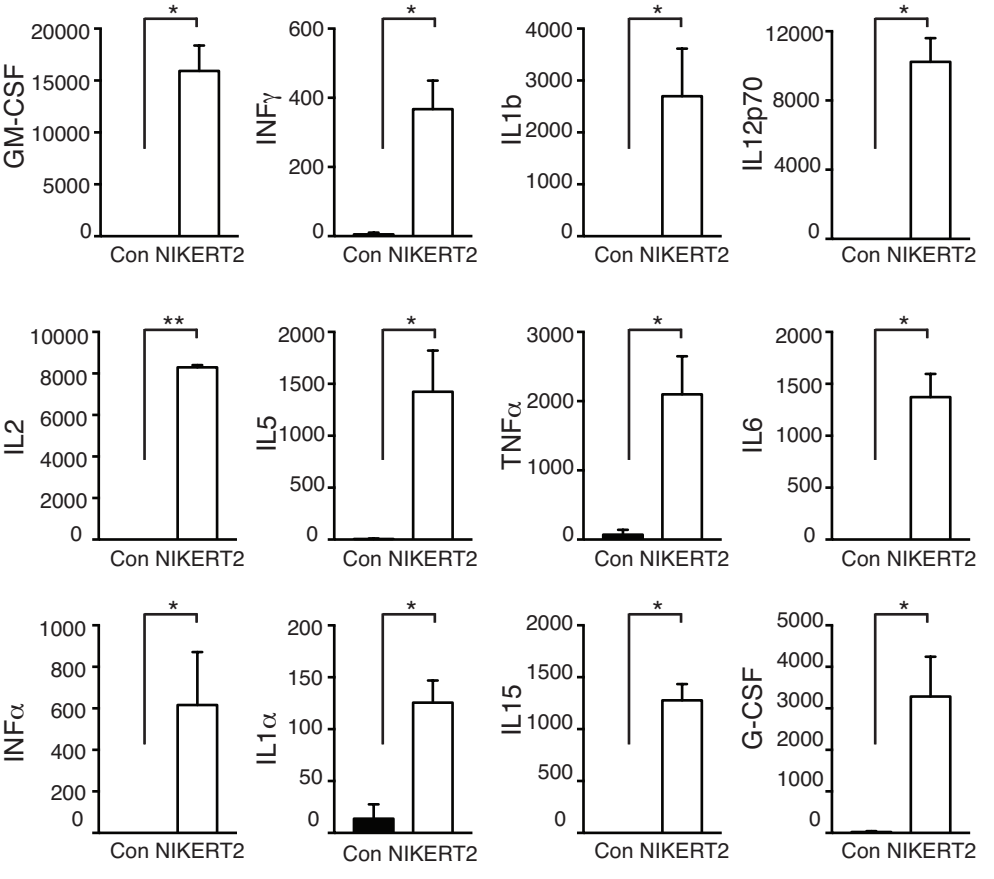

Supplemental Fig. 2 Zhao et al.

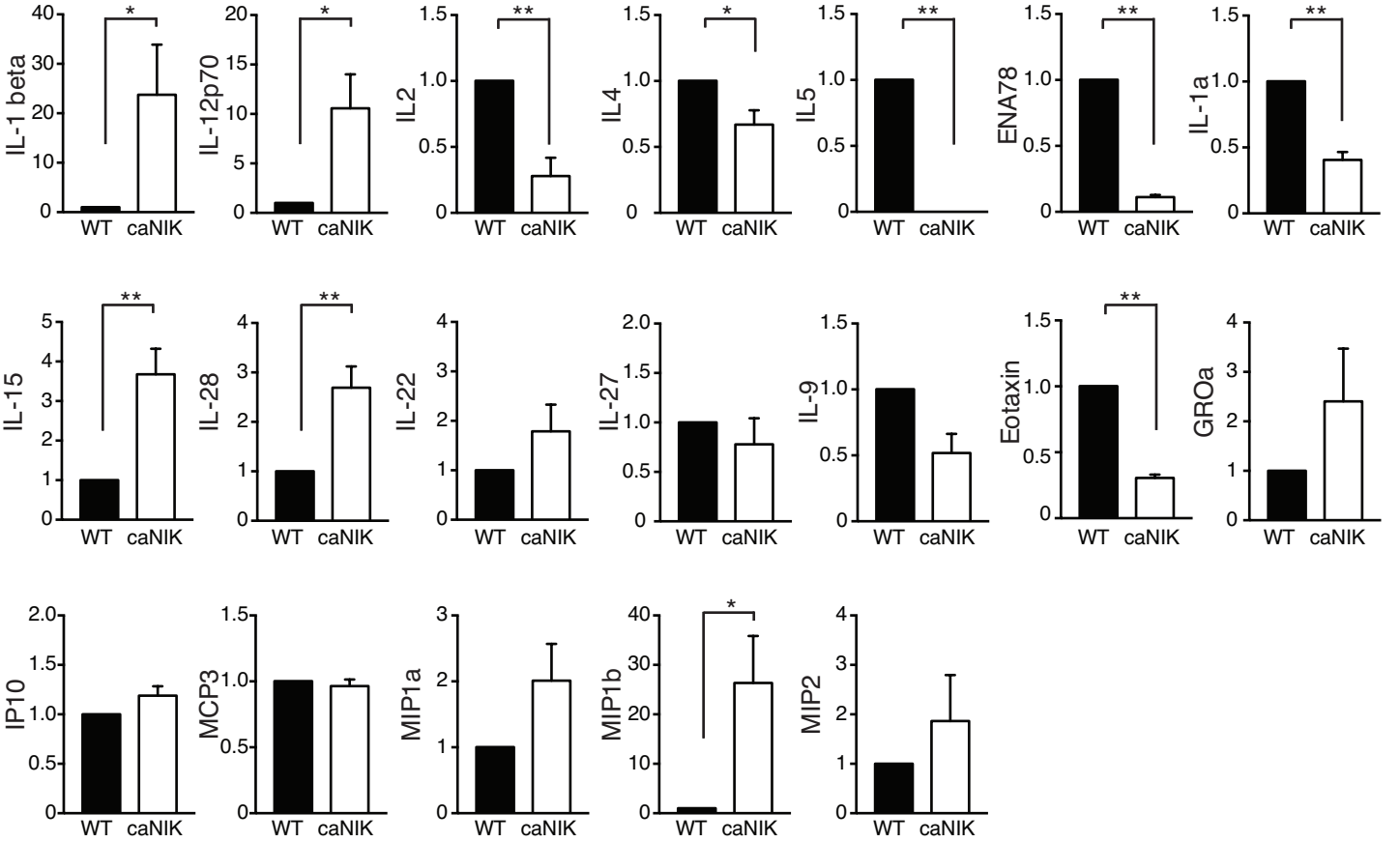

Supplemental Fig. 3 Zhao et al.

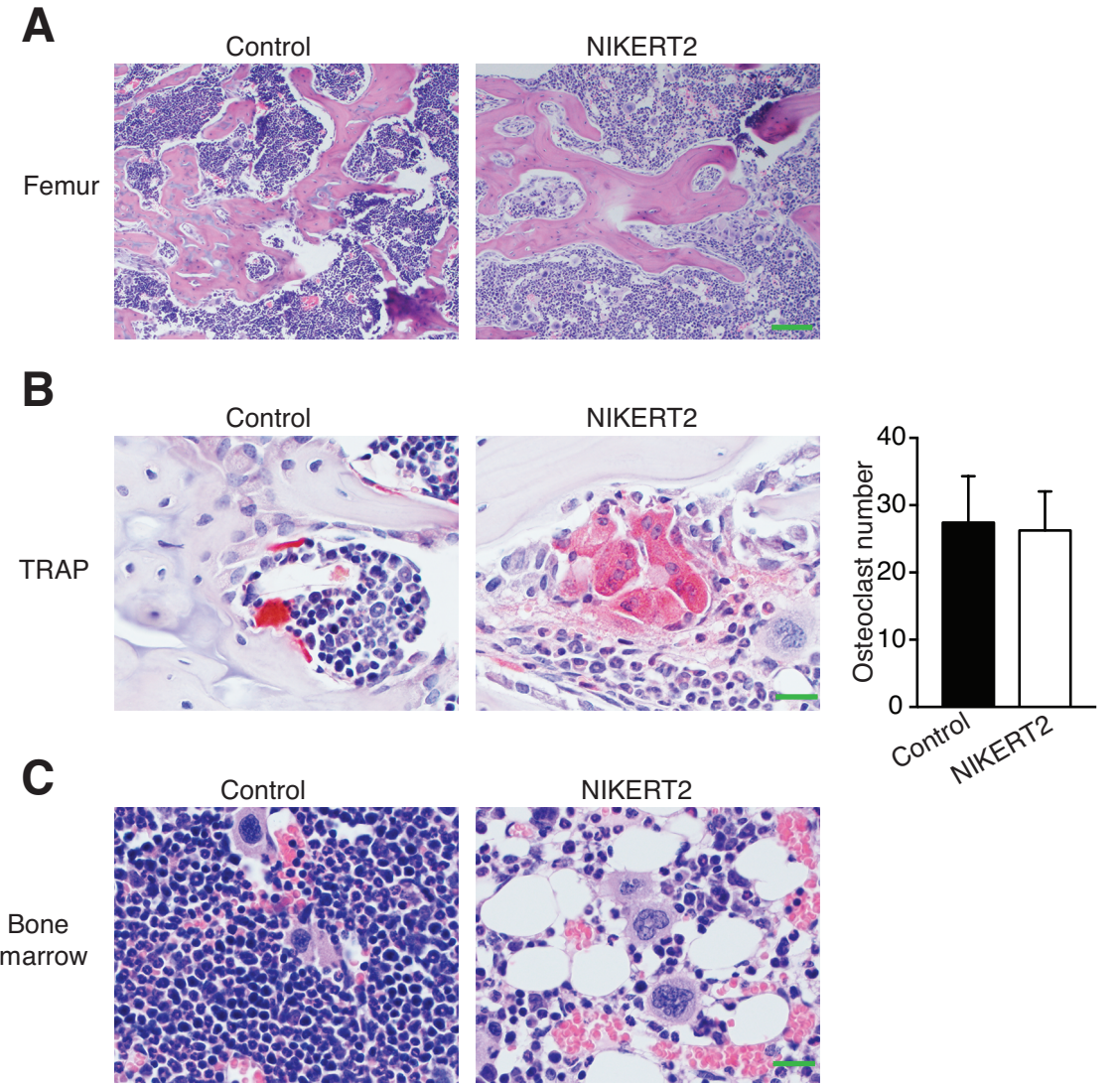

Supplemental Fig. 4 Zhao et al.

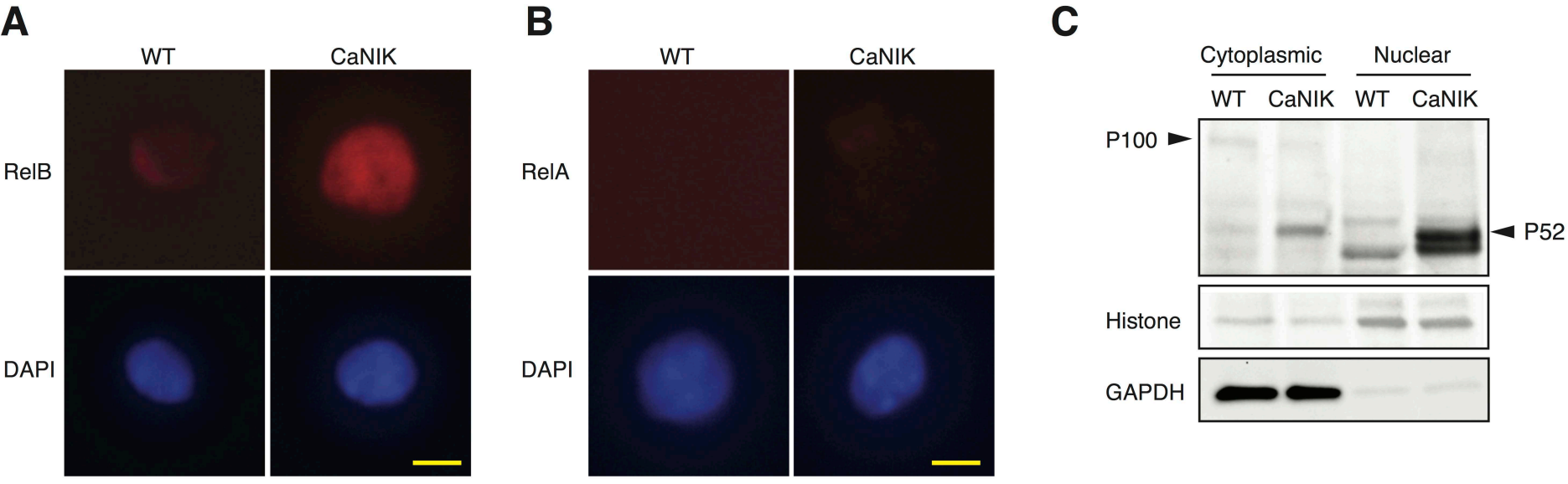

Supplemental Fig. 4 Zhao et al.

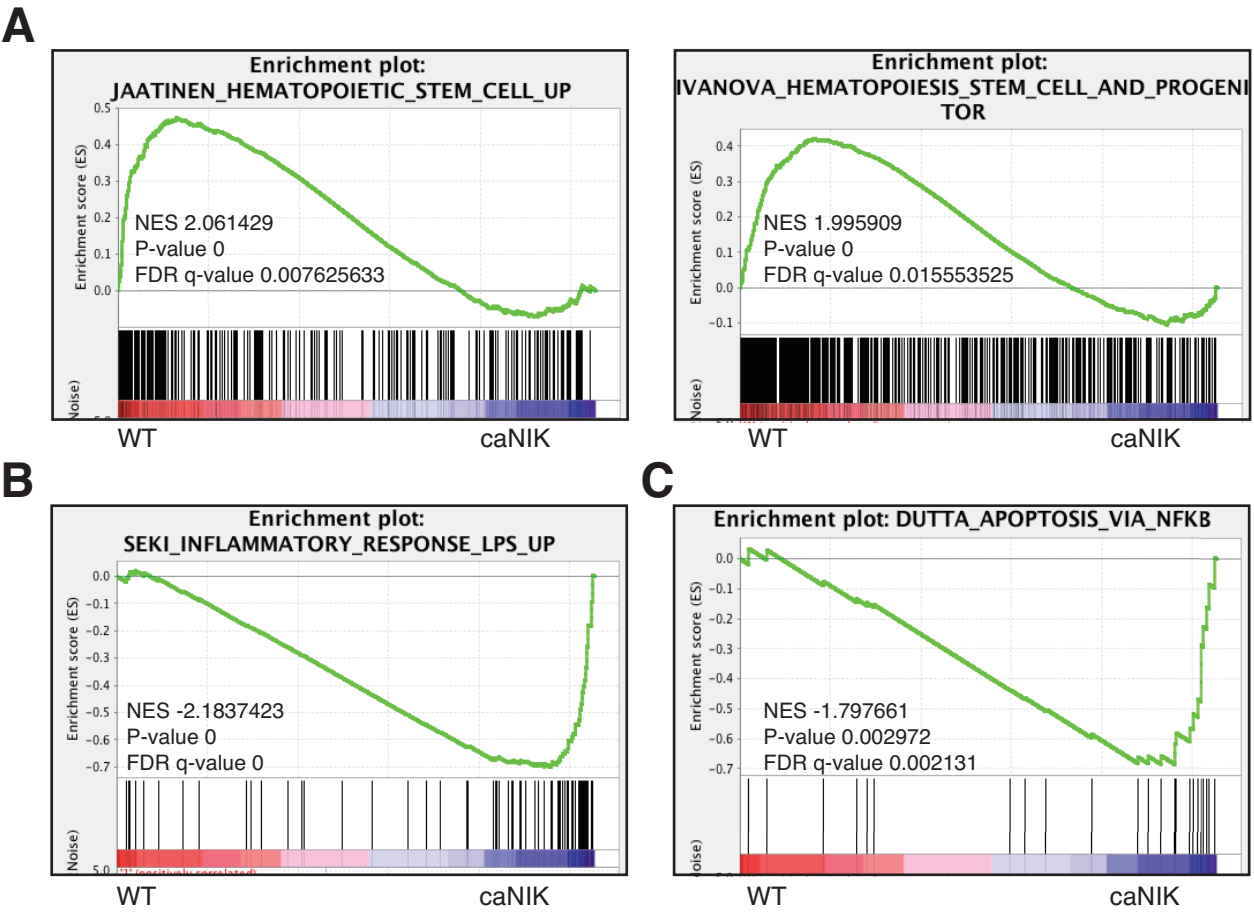

Supplemental Fig. 5 Zhao et al.

Supplemental Figure Legends

Supplemental Figure 1. NIK-activated HSPCs are functionally impaired. Sorted Lin^- $cKit^+Sca1^+$ HSPCs ($CD45.2^+$, 2500/recipient) from WT or caNIK mice were transplanted together with radioprotective cells (45.1^+, 2×10^5/recipient) into lethally irradiated congenic recipients ($CD45.1^+$). (**A**) FACS plots show representative donor-derived chimerism from recipients receiving WT or caNIK KLS cells16 weeks post-BMT. (**B**) Donor-derived chimerisms at 16 weeks post-BMT (six recipients receiving WT KLS cells and eight receiving caNIK KLS cells, *$p<0.05$). Each dot represents one individual recipient.

Supplemental Figure 2. Systemic NIK activation induces inflammatory cytokine "storm". Mouse serum was prepared by centrifugation of clotted mouse peripheral blood from control or tamoxifen-treated NIKERT2 (n=4) mice and the cytokines were measured using ProcartaPlex Mouse Cytokine & Chemokine Panel 1A (36 plex) (*$p<0.05$, **$p<0.01$). The expression of IL13, IL4, ENA78, IL28, IL31, LIF, M-CSF, IL10, IL17a, IL22, IL27, IL9, Eotaxin, GROa, IP10, MCP1, MCP3, MIP1a, MIP1b, MIP2 and RANTEs was also elevated (data not shown).

Supplemental Figure 3. NIK activation up-regulates inflammatory cytokines. Mouse serum was prepared by centrifugation of clotted mouse peripheral blood from WT (n=4) or caNIK (n=7) mice and the cytokines were measured using ProcartaPlex Mouse Cytokine & Chemokine Panel 1A (36 plex) (*$p<0.05$, **$p<0.01$). The expression of GM-

CSF, IL10, IL13, IL17a, IL31, INFa, LIF, MCP1, M-CSF and RANTES was undetectable.

Supplemental Figure 4. Systemic activation of NIK alters BM microenvironment. (**A**) H&E stains of femurs from control or NIKERT2 mice three days after the last tamoxifen treatment (n=5). Note the decreased trabecular bone volume and osteoclast clusters in NIKERT2 femurs. Scale bar 100 μm. (**B**) Left, TRAP stains of femurs from control or NIKERT2 mice three days after the last tamoxifen treatment. Scale bar 20μm; Right, average number of osteoclasts (mean ± sem.) with two or more nuclei per cross-section (n=5). (**C**) Increased adipose tissue in tamoxifen-treated NIKERT2 bone marrow. Scale bar 20μm.

Supplemental Figure 5. Increased nuclear localization of RelB and p52 in NIK activated bone marrow cells. Immunofluorescence staining of RelB (Santa Cruz, sc-226) (**A**) or RelA (Cell signaling Technology #8242) (**B**) using sorted KLS cells from WT and caNIK mice. Nuclei were counterstained with DAPI. Scale bar 5 μm. (**C**) Accelerated p100 processing and nuclear translocation by NIK activation. 50μg of denatured cytoplasmic or nuclear proteins extracted from control or NIK lineage$^-$ BM cells using (NEPERNuclear and Cytoplasmic extraction reagent, ThermoScientific #78833) were run on 4-15% gel and immunoblotted with p100 antibody (Cell Signaling #4882) first, then re-probed with anti-histone H3 (Cell Signaling #4499) and anti-GAPDH (Santa Cruz sc-32233) for nuclear and cytoplasmic loading controls, respectively.

Supplemental Figure 6. NIK activation induces increased inflammatory response signature, decreased HSPC signatures and increased apoptotic signatures.

Gene set enrichment analysis (GSEA) of statistically significant gene sets enriched in the KLS cells of caNIK mice (up in caNIK) or WT mice (down in caNIK).